Structural Basis for p300 Taz2-p53 TAD1 Binding and Modulation by Phosphorylation

11 AUTHORS, INCLUDING:

Sharlyn J Mazur
U.S. Department of Health and Human Services

47 PUBLICATIONS **1,814** CITATIONS

SEE PROFILE

Maria Miller
National Institutes of Health

62 PUBLICATIONS **3,983** CITATIONS

SEE PROFILE

Ettore Appella
National Institutes of Health

214 PUBLICATIONS **16,210** CITATIONS

SEE PROFILE

Structural Basis for p300 Taz2/p53 TAD1 Binding and Modulation by Phosphorylation

Hanqiao Feng[1,†], **Lisa M. Miller Jenkins**[2,†], **Stewart R. Durell**[2], **Ryo Hayashi**[2], **Sharlyn J. Mazur**[2], **Scott Cherry**[3], **Joseph E. Tropea**[3], **Maria Miller**[3], **Alexander Wlodawer**[3], **Ettore Appella**[2,*], and **Yawen Bai**[1,*]

[1]Laboratory of Biochemistry and Molecular Biology, National Cancer Institute, NIH, Bethesda, MD 20892, U.S.A.

[2]Laboratory of Cell Biology, National Cancer Institute, NIH, Bethesda, MD 20892, U.S.A.

[3]Macromolecular Crystallography Laboratory, National Cancer Institute at Frederick, Frederick, Maryland 21702, U.S.A.

Summary

Coactivators CBP and p300 play important roles in mediating the transcriptional activity of p53. Until now, however, no detailed structural information has been available on how any of the domains of p300 interact with p53. Here, we report the NMR structure of the complex of the Taz2 (C/H3) domain of p300 and the N-terminal transactivation domain of p53. In the complex, p53 forms a short α-helix and interacts with the Taz2 domain through an extended surface. Mutational analyses demonstrate the importance of hydrophobic residues for complex stabilization. Additionally, they suggest that the increased affinity of Taz2 for $p53_{1-39}$ phosphorylated at Thr_{18} is due in part to electrostatic interactions of the phosphate with neighboring arginine residues in Taz2. Thermodynamic experiments revealed the importance of hydrophobic interactions in the complex of Taz2 with p53 phosphorylated at Ser_{15} and Thr_{18}.

The tumor suppressor p53 is a central transcription factor that integrates many stress signals following DNA damage, resulting in transcriptional activation of key genes involved in cell cycle arrest and apoptosis (Das et al. 2008). Its functional activity is initiated in part by site-specific recruitment of the histone acetyltransferase coactivators CREB-binding protein (CBP) and p300, which promote local chromatin unwinding (Barlev et al. 2001, Liu et al. 2003). In addition, CBP and p300 acetylate p53 on six C-terminal lysine residues; these modifications further stabilize and activate the protein (Gu and Roeder 1997, Ito et al. 2001, Sakaguchi et al. 1998).

CBP and p300 are paralogs composed of seven distinct domains arranged in a common architecture. Among those domains are two transcriptional adaptor zinc-binding (Taz) domains, Taz1 (C/H1) and Taz2 (C/H3), which mediate protein-protein interactions important

for the transcriptional coactivator functions of these proteins. Taz1 has been found to interact with HIF-1α and CITED2, while Taz2 binding partners include E1A, GATA-1, and E2F (Goodman and Smolik 2000). Furthermore, both domains have been shown to interact with p53 through its N-terminal transactivation domain (TAD) (Avantaggiati et al. 1997, Grossman et al. 1998). The p53 TAD can be divided into two subdomains, TAD1 composed of residues 1-40 and TAD2 composed of residues 41-61, which can independently activate transcription (Candau et al. 1997). TAD1 has been shown to interact with both Taz1 and Taz2 of p300 (Polley et al. 2008, Teufel et al. 2007). TAD2 plays a role in binding to Taz1 (Polley et al. 2008), and we recently determined that TAD2 is also able to interact with Taz2 with an affinity similar to that observed for TAD1 (Jenkins et al. 2009 Biochemistry DOI:10.1021/bi801716h).

In response to DNA damage-inducing stress, the p53 TAD may be phosphorylated at up to 10 different sites by multiple kinases (Appella and Anderson 2001). These modifications disrupt MDM2 binding, thereby preventing ubiquitylation and degradation of p53 (Bottger et al. 1999, Craig et al. 1999). The post-translational modifications have also been shown to modulate the interaction of p53 with other proteins. For example, binding of p53 to MDM2 is weakened by phosphorylation of Thr_{18} (Sakaguchi et al. 2000), while its binding to the p62 subunit of TFIIH is strengthened by phosphorylation of Ser_{46} and Thr_{55} (Di Lello et al. 2006). In addition, we and others have recently demonstrated that phosphorylation of p53 increases its affinity for p300, including binding to the Taz1 and Taz2 domains (Polley et al. 2008) (Jenkins et al. 2009 Biochemistry DOI:10.1021/bi801716h).

The recruitment of p300 to gene promoters by p53 is critical for the transactivation activity of p53. Chromatin-bound p53 recruits p300 to the promoter, resulting in localized acetylation of histones, thereby facilitating transcription (Espinosa and Emerson 2001). The amount of p300 binding by p53 correlates with the extent of histone acetylation and the induction of p53-dependent transcription (Liu et al. 2003). Inhibition of binding by competitor proteins or down-regulation of CBP or p300 by siRNA has been found to repress p53-mediated transcription and reduce local histone acetylation at p53 promoters (Hsu et al. 2004, Liu et al. 2003, Luo et al. 2001, Vaziri et al. 2001). Furthermore, the interaction between p53 and the Taz2 domain of p300 is especially important, as it has been shown that catalytically-inactive deletion mutants of p300 containing this domain can dominantly inhibit p53-dependent apoptosis and G1 arrest (Avantaggiati et al. 1997, Scolnick et al. 1997). Thus, the interaction between p53 and p300 is central to the transcriptional activity of p53.

To better understand the molecular determinants of the interaction between p53 TAD1 and Taz2, we have used NMR spectroscopy to determine the solution structure of the complex of these two proteins. The structure reveals the importance of key hydrophobic interactions in stabilizing the complex; fluorescence anisotropy binding experiments further demonstrate the requirement for specific residues for binding. In addition, isothermal titration calorimetry (ITC) and chemical shift mapping were used to characterize the binding of phosphorylated forms of p53 to Taz2. These experiments suggest the importance of hydrophobic and specific electrostatic interactions in the stabilization of the p300-p53 complex through phosphorylation of p53.

Results

Structure Determination of the Taz2/p53$_{2-39}$ Complex

Molecular determinants of the interaction of the human p300 Taz2 domain with p53 TAD1 were investigated in 2D ^{1}H,^{15}N-HSQC experiments in which unlabeled p53$_{2-39}$ was titrated into ^{15}N-labeled Taz2. Under the same conditions that were used in an earlier study for the titration of p53$_{14-28}$ into ^{15}N-labeled CBP Taz2 (De Guzman et al. 2000), many Taz2 amide peaks disappeared (see Figure S1 available online). A similar loss of amide signals was reported

for the titration of p300 Taz2 into ^{15}N-labeled $p53_{1-57}$ (Teufel et al. 2007). To search for conditions that could restore the amide resonances, we varied the pH, salt concentration, and temperature of the samples and monitored the 2D $^1H,^{15}N$ HSQC spectrum of Taz2. Under the optimized conditions (35 °C, 50 mM MES pH 6.3, 200 mM NaCl, 0.1 mM ZnCl, 1 mM DTT), nearly all Taz2 amide cross peaks were observed (Figure S1).

Under the optimal conditions described above, we determined the solution structure of the complex by NMR methods using isotope-labeled Taz2 or $p53_{2-39}$ proteins. The 3D structures of the complex were calculated with 1732 NOE-derived distance constraints, 94 hydrogen bonds, 229 dihedral angle restraints, and 52 intermolecular NOEs between Taz2 and $p53_{2-39}$. The structure of Taz2 in the complex is well defined, whereas only residues 15-27 of $p53_{2-39}$ are well defined (Figure 1A and Table 1). The RMSDs for the backbone and all heavy atoms in the folded regions are 0.31 Å and 0.56 Å, respectively. Less defined regions in $p53_{2-39}$ showed large dynamic motions, as illustrated by the low values of heteronuclear $^{15}N\text{-}\{^1H\}$ NOEs (Figure 1B), indicating that the less defined structure in these regions is an intrinsic feature of the complex. The calculated structures were further verified by examining the effect of mutations and side-chain modifications of p53 on the amide ^1H and ^{15}N chemical shifts in Taz2, including $p53_{9-33}$(L14A), $p53_{9-33}$(L22A), $p53_{9-33}$(L26A), $p53_{9-33}$(E28Q), $p53_{9-33}$(N29D), $p53_{9-33}$(N30D), and $p53_{9-33}$(V31C-MTSSL). These mutations and modifications have significant effects only on the amide ^1H and ^{15}N chemical shifts or cross-peak intensities of Taz2 residues that are proximal to the p53 modification sites in the calculated structures.

Overall Structure of the Complex

In the complex, the p300 Taz2 domain forms four core α-helices with three HCCC-type zinc-binding motifs (Figure 1C). In addition, a very short helix is observed between helices α2 and α3. The structure of Taz2 in this complex is very similar to the structure of free CBP Taz2 (De Guzman et al. 2000). The backbone RMSD between the structure of free CBP Taz2 and the p300 Taz2-$p53_{2-39}$ complex is 2.0 Å. Alignment of helices 1-3 of the free CBP Taz2 and p300 Taz2 complex resulted in a backbone RMSD of 1.2 Å. Whereas free $p53_{2-39}$ displays a highly flexible conformation in solution, it forms a short α-helical conformation within residues 15-27 in complex with Taz2. Chemical shift analysis revealed that the largest changes in bound p53 compared with a random coil (Wishart et al. 1995) were in residues 17-24 (Figure 1D). The helical region of p53 interacts with helices $α_1$, $α_2$, and $α_3$ of Taz2 (Figure 1C). This binding site corresponds to the site identified previously through chemical shift mapping for $p53_{14-28}$ binding to CBP Taz2 (De Guzman et al. 2000). Complex formation results in a 2300 Å^2 reduction in the solvent-accessible surface area, with a reduction of 1100 Å^2 of polar surface area and 1200 Å^2 of non-polar surface area.

Interactions between Taz2 and $p53_{2-39}$ at the Interface

At the Taz2-$p53_{2-39}$ interface, interactions were observed primarily between hydrophobic amino acids with some additional contributions from charged and polar residues. Phe_{19} of p53 is nestled between the hydrophobic parts of the side chains of Arg_{1737} and Lys_{1760} in Taz2 (Figure 2A). The position of the side chain of Arg_{1737} differs significantly between the free CBP Taz2 and the complex with $p53_{2-39}$. In CBP Taz2, the side chain was found to be flexible among the ensemble of structures, whereas in the complex, it is less flexible and its orientation along the p53 helix is maintained by interaction with the aromatic ring of Phe_{19}. In addition, we observed that the amide ^1H and ^{15}N resonances of this residue were highly shifted upon titration of $p53_{2-39}$ (data not shown). The positively charged amine group on the side chain of Lys_{1760} may be stabilized by the π electrons of the aromatic ring of Phe_{19}. The Cα and Cβ of Leu_{22} form non-polar interactions with the side chain of Val_{1764} and Sδ of Met_{1761}. Additionally, the Leu_{22} side chain forms contacts with Cε of Lys_{1760}. The Cα of Leu_{25} contacts

$C\gamma1$ and $C\delta$ of Ile_{1781}, while the $C\delta1$ and $C\delta2$ of Leu_{25} contact the side chain of Pro_{1780} (Figure 2A). The methyl group of Thr_{18} of p53 is located in a hydrophobic environment made up of the aliphatic portion of Taz2 Gln_{1784} and Ala_{1738}, Leu_{1785}, and Leu_{1788}.

The importance of the hydrophobic interactions for the $p53_{2-39}$-Taz2 complex was further demonstrated by analysis of Taz2 binding to a series of p53 peptides in which a selected hydrophobic amino acid was replaced by alanine. Fluorescence anisotropy assays were used to determine the dissociation constants for the binding of p53 peptides to Taz2 by competition with fluorescein-labeled $p53_{14-28}$. No measurable Taz2 binding was observed for alanine mutants of Phe_{19}, Leu_{22} or Leu_{25}, three hydrophobic p53 residues that directly contact Taz2. In contrast, when Leu_{26}, whose side chain projects away from Taz2 in the complex, was mutated to alanine, the observed dissociation constant ($K_d = 13.6 \pm 4.0$ μM) was similar to that of the wild type sequence ($K_d = 17.6 \pm 4.4$ μM). The observed binding affinities confirm the importance of specific hydrophobic residues in Taz2-$p53_{2-39}$ complex formation.

Electrostatic interactions were also apparent at the Taz2-$p53_{2-39}$ interface. The p53 binding site of Taz2 has areas of positive charge along the flexible residues N-terminal and C-terminal to the helix (Figure 2B). In most of the calculated structures, the carboxylate side chain of p53 Glu_{11} contacted the guanidinium group of Taz2 Arg_{1731} (2.5-4.8 Å apart among the 10 lowest-energy structures) (Figure 2C). As this residue of p53 is flexible, this interaction may be transient. However, the observation of intermolecular NOEs between Taz2 and p53 residues in the flexible regions from 9-14 and 28-31 suggests that these interactions do take place. Furthermore, large changes in $C\alpha$ chemical shifts were also observed for residues 10, 11, 14, and 15 of p53 upon complex formation. A salt bridge was observed between Taz2 Arg_{1731} and p53 Glu_{17} (3.2-4.2 Å). Specific polar interactions were seen between the side chains of p53 Asp_{21} and Taz2 Gln_{1784} (3.1-5.0 Å), the hydroxyl group on the side chain of p53 Thr_{18} and side chain hydroxyl of Taz2 Ser_{1734} (2.4-2.5 Å), the hydroxyl group of p53 Ser_{15} and the side chain of Arg_{1737} (3.4-7.8 Å), and the side chain of p53 Glu_{17} and the hydroxyl of Taz2 Ser_{1734} (3.5-4.1 Å).

As we found that p53 TAD1 and TAD2 bind to Taz2 with similar affinities (Jenkins et al. 2009 Biochemistry DOI:10.1021/bi801716h), we next used 2D ^{1}H, ^{15}N HSQC experiments to explore the binding site of p53 TAD2 on Taz2. Titration of $p53_{35-59}$ into ^{15}N-labeled Taz2 revealed significant chemical shift changes for multiple amide resonances of Taz2 (Figure S2A). Some of the affected residues were similarly shifted upon titration of $p53_{2-39}$ into ^{15}N-labeled Taz2 (Figure S2B), suggesting that TAD1 and TAD2 have overlapping binding sites on Taz2.

Modulation of the Interactions between Taz2 and p53 TAD1 by Phosphorylation

An important aspect of the interaction between Taz2 and p53 TAD1 is the modulation of the binding affinity by phosphorylation. Among the residues of p53 at the interface are two important sites of phosphorylation, Ser_{15} and Thr_{18}. In the complex, the methyl of the Thr_{18} side chain is in a local hydrophobic environment while the targeted hydroxyl forms a hydrogen bond with Ser_{1734} (Figure 2C). Likewise, the targeted hydroxyl of Ser_{15} is proximal to the side chain of Arg_{1737}. The local environments of Ser_{15} and Thr_{18} suggest that phosphorylation of these residues may alter the balance of hydrophobic and electrostatic interactions in the complex. To investigate these effects in detail, ITC experiments were performed in which p53 phosphorylated at Ser_{15}, Thr_{18} or both sites was titrated into Taz2 at 15, 25, and 35 °C.

Titration of $p53_{1-39}Ser15p$ into Taz2 at 35 °C was fit by a 1:1 binding model (Figure S3). The binding was exothermic and was characterized by the dissociation constant $K_d = 0.96$ μM (Table 2). This value is approximately three times higher than that observed for $p53_{1-39}$ ($K_d = 2.7$ μM), and the change in enthalpy is 1.2 kcal/mol greater for the phosphorylated form than

the non-phosphorylated form (Jenkins et al. 2009 Biochemistry DOI:10.1021/bi801716h). Similarly, $p53_{1-39}$Thr18p was titrated into Taz2 at 35 °C (Figure S3). The binding of $p53_{1-39}$Thr18p was exothermic, similar to that of $p53_{1-39}$Ser15p (Table 2). The affinity of Taz2 for $p53_{1-39}$Thr18p was 11-times greater than that of $p53_{1-39}$ and 4-times greater than that of $p53_{1-39}$Ser15p (Table 2). Finally, the diphosphorylated peptide, $p53_{1-39}$Ser15p, Thr18p was titrated into Taz2 at 35 °C (Figure S3). The binding of $p53_{1-39}$Ser15p, Thr18p to Taz2 was also exothermic, although the magnitude was smaller than that observed for any other form of $p53_{1-39}$. The affinity was intermediate to that of the two monophosphorylated forms and approximately seven times larger than non-phosphorylated $p53_{1-39}$ (Table 2). This result suggests that the stabilization produced by diphosphorylation at Ser_{15} and Thr_{18} is less than the additive effects of the individual phosphorylations.

At 15 °C, complex formation by each of the three phosphorylated forms is endothermic, whereas, at 25 °C, all are close to zero (Table 2). The magnitude of ΔH at 15 °C is greatest for $p53_{1-39}$Ser15p and $p53_{1-39}$Thr18p, followed by the non-phosphorylated form; it is the smallest for $p53_{1-39}$Ser15p, Thr18p. The value of the heat capacity at constant pressure, ΔC_p, is similar for the interactions between Taz2 and $p53_{1-39}$Ser15p and $p53_{1-39}$Thr18p (Table 2); these values are 25-30% more negative than the ΔC_p for the interaction of Taz2 with $p53_{1-39}$ observed previously (Jenkins et al. 2009 Biochemistry DOI:10.1021/bi801716h). Hydrophobic and polar interactions are thought to contribute to the ΔC_p with opposing signs; thus, a negative ΔC_p suggests that the binding is dominated by hydrophobic interactions (Baldwin 1986,Livingstone et al. 1991,Prabhu and Sharp 2005). The more negative value of ΔC_p for the binding of $p53_{1-39}$Ser15p and $p53_{1-39}$Thr18p to Taz2 suggests that the extent of hydrophobic interactions is increased in these complexes compared to the complex with the non-phosphorylated peptide. Interestingly, although ΔC_p for the interaction between Taz2 and $p53_{1-39}$Ser15p, Thr18p is still negative, the magnitude is only about 45% that for the formation of the complex with either monophosphorylated peptide (Table 2). This value suggests a different composition of hydrophobic and electrostatic interactions in the complex of Taz2 with diphosphorylated p53 TAD1.

ITC experiments were performed at lower and higher salt concentrations to examine ionic contributions to the binding of $p53_{1-39}$ and phosphorylated forms for Taz2. Compared to the affinities observed at 100 mM NaCl, the binding of $p53_{1-39}$ and phosphorylated forms were 5 to 10-times tighter at 50 mM NaCl and correspondingly weaker at 200 mM NaCl (Table 3). The dependence of the binding affinity on salt concentration provides information about the net difference in the number of thermodynamically-involved ions upon complex formation. This analysis suggests that complex formation between $p53_{1-39}$ and Taz2 releases approximately 2 thermodynamically involved ions, whereas complex formation between Taz2 and $p53_{1-39}$Ser15p or $p53_{1-39}$Ser15p, Thr18p results in the release of approximately 3 thermodynamically bound ions. Interestingly, only approximately 2 thermodynamically-involved ions are released upon binding of $p53_{1-39}$Thr18p, which is similar to the value for binding the non-phosphorylated peptide. Extrapolation of the binding constants to 1 M NaCl allows an estimate of the affinity without the contribution from the release of thermodynamically-involved ions. The extrapolated association constants for complex formation with $p53_{1-39}$, $p53_{1-39}$Ser15p and $p53_{1-39}$Ser15p, Thr18p are similar, with the value for $p53_{1-39}$Ser15p being 1.4-fold larger. In contrast, the extrapolated association constant for $p53_{1-39}$Thr18p is approximately five times larger than for the unmodified form, suggesting greater differences in the binding of this phosphorylated form. Thus, although at moderate salt concentrations, the stabilization resulting from the release of thermodynamically-involved ions is similar for the Taz2-$p53_{1-39}$Ser15p and Taz2-$p53_{1-39}$Thr18p complexes, the increased affinity of $p53_{1-39}$Thr18p for Taz2 observed at 0.1 M NaCl reflects a larger contribution from additional stabilizing interactions.

Two dimensional ^{1}H, ^{15}N HSQC spectra were collected to further characterize the effects of Thr$_{18}$ phosphorylation in the Taz2-p53$_{2-39}$ complex. Titration of p53$_{1-39}$Thr18p into ^{15}N-labeled Taz2 produced extensive changes in chemical shifts. Chemical shift mapping demonstrated significant changes in the amide resonances of Leu$_{1733}$, Ile$_{1735}$, Ala$_{1738}$, Gln$_{1740}$, Ser$_{1741}$, Leu$_{1742}$, and Gln$_{1784}$ of Taz2, with smaller changes observed for Ile$_{1739}$, Lys$_{1760}$, and Leu$_{1785}$ (Figure 3, S4). Due to the overlap in the ^{1}H,^{15}N HSQC spectra, we were unable to determine whether the amide chemical shift of Arg$_{1731}$ or Arg$_{1732}$ of Taz2, two basic residues proximal to the modification site, changed upon addition of the phosphorylated peptide. The results of the chemical shift mapping thus suggest a rearrangement of residues at the hydrophobic interface, consistent with the thermodynamic results for binding of Taz2 to p53$_{1-39}$Thr18p.

In the Taz2/p53$_{2-39}$ complex, Ser$_{15}$ of p53 is proximal to Arg$_{1737}$ of Taz2 and, as stated above, Thr$_{18}$ of p53 is proximal to Arg$_{1731}$ and Arg$_{1732}$ of Taz2 (Figure 2C). To explore the possible role of these arginine residues in stabilization of the phosphorylated forms of p53, we separately mutated to alanine each of these three residues of Taz2 (Arg$_{1731}$, Arg$_{1732}$, and Arg$_{1737}$) that are closest to p53 Ser$_{15}$ and Thr$_{18}$ in the complex. The CD spectra of all three mutant Taz2 proteins were similar to that of the parent protein, suggesting that the proteins folded similarly (Figure S5). The binding of the mutant peptides were then examined by ITC at 35 °C. All three mutant Taz2 proteins bound non-phohsphorylated p53$_{1-39}$ with similar affinities as Taz2 (Table 4). Surprisingly, the binding affinity of Taz2(R1737A) to p53$_{1-39}$Ser15p was approximately four-fold greater than to the non-phosphorylated form (Table 4), similar to the binding of this peptide to Taz2. Although p53 Ser$_{15}$ and Taz2 Arg$_{1737}$ are close to one another in the structure, Ser$_{15}$ is located in a flexible region of p53, so this residue may be able to be stabilized by a different residue in the Taz2(R1737A) mutant or the phosphorylated protein may bind in a different manner than does the non-phosphorylated peptide. In contrast, Taz2(R1731A) and Taz2(R1732A) bound p53$_{1-39}$Thr18p 5.5-times more tightly than the non-phosphorylated form (Table 4). This binding is two times weaker than observed for the binding of Taz2 to p53$_{2-39}$Thr18p, suggesting that both Arg$_{1731}$ and Arg$_{1732}$ play a role in stabilization of p53$_{1-39}$Thr18p, consistent with their proximity to Thr$_{18}$ in the complex. The lack of a larger difference in binding by the two mutants may be due to stabilization of the phosphorylation by the alternate arginine residue or a difference in binding of the non-phosphorylated and phosphorylated peptides.

Discussion

The p53 TAD has been described as intrinsically disordered (Dunker et al. 2005). Frequently, intrinsically disordered protein domains are able to take on a number of conformations, particularly in complex with other proteins, to effect different biological outcomes (Vise et al. 2007). In the free form, the TAD of p53 is flexible and unstructured. Recently, it has been demonstrated that TAD1 forms a dynamic α-helix, while two turns can be observed within TAD2 (Lee et al. 2000, Vise et al. 2005). This dynamic structure allows p53 to be involved in a variety of cellular responses by conforming to the proteins with which it interacts. In four previously determined structures of p53 TAD peptides in complex with proteins, both TAD1 and TAD2 have been found to form short α-helices and the binding was shown to be mediated by hydrophobic interactions (Bochkareva et al. 2005, Di Lello et al. 2006, Kussie et al. 1996, Popowicz et al. 2008).

The complex of p53 TAD1 with Taz2 is similar to the complexes formed with MDM2 and MDMX, in which p53$_{18-26}$ forms an amphipathic helix. Although hydrophobic interactions are important in all three interfaces, the specific residues involved in the interactions differ. In the MDM2 and MDMX complexes, Phe$_{19}$, Trp$_{23}$, and Leu$_{26}$ form the primary hydrophobic interactions, whereas in the Taz2 complex, we find that Phe$_{19}$, Leu$_{22}$, and Leu$_{25}$ are the most

critical. Indeed, Trp_{23} and Leu_{26} project away from Taz2, whereas Leu_{25} projects away from MDM2 (Figure S6). We further observed that mutation of Leu_{26}, important for MDM2 binding, did not affect binding of p53 to Taz2. In addition, although it is not buried in the hydrophobic pocket on MDM2 (Figure S6B), p53 Leu_{22} makes hydrophobic interactions that stabilize the complex (Kussie et al. 1996). As observed for p53 binding to Taz2, mutation of Leu_{22} to alanine also disrupts binding of p53 to MDM2 (Picksley et al. 1994). Although both complexes involve binding to α-helical regions of p53, the binding of p53 to MDM2 requires a shorter segment of p53 and has a higher affinity. In contrast, we found that the binding of p53 to Taz2 is approximately an order of magnitude weaker (K_d = 0.4 μM for binding to MDM2 and 3 μM for binding to Taz2) and involves a longer region of p53. The structure of the p53/MDM2 complex shows that p53 fits into a deep hydrophobic cleft on MDM2, with key hydrophobic residues buried in the interface. Although the interaction with Taz2 also involves hydrophobic interactions, p53 lies across the surface of Taz2 formed by helices α1, α2, and α3. The extended interaction site of p53 TAD1 on Taz2 is reflected in the greater loss of solvent-accessible surface area for this complex than that calculated for the MDM2-$p53_{15-29}$ complex (Kussie et al. 1996). The Taz2-$p53_{2-39}$ complex shares common features with other complexes of intrinsically disordered domains, including large interaction area, large exposed surface area per residue, and binding through a single continuous segment of the protein (Meszaros et al. 2007). Based upon the observed changes in polar and non-polar solvent accessible surface area upon Taz2-$p53_{2-39}$ complexation, we estimated ΔCp for complex formation to be -244 cal/mol·K (Loladze et al. 2001). This value is very similar to value of ΔCp determined from thermodynamic measurements (Jenkins et al. 2009 Biochemistry DOI:10.1021/bi801716h).

Our structural and binding studies allow better understanding of the molecular basis for the increased binding affinity between Taz2 and $p53_{1-39}$ upon phosphorylation at Ser_{15} and Thr_{18}. In the Taz2-$p53_{2-39}$ complex, p53 Ser_{15} and Thr_{18} are located in a basic environment on Taz2 (Figure 2); thus, phosphorylation at these sites contributes to increased affinity through stabilizing interactions. Similarly, it has been suggested that the decreased affinity of phosphorylated p53 for MDM2 is due to a local acidic environment near Thr_{18} and Ser_{20} on MDM2 that repels these residues when phosphorylated (Lee et al. 2007). As phosphorylation has been suggested to stabilize helical conformation when it occurs at the N-terminus (Smart and McCammon 1999), modification of Ser_{15} may also stabilize the p53 helix, thereby increasing the affinity for Taz2. Although Arg_{1731} and Arg_{1732} play a role in stabilization of phosphorylation at Thr_{18} (Table 4), the more negative ΔCp for the modified form compared to the non-phosphorylated form (Table 2) suggests that, consistent with changes observed in the chemical shift mapping experiments, the extent of hydrophobic interactions increased for $p53_{1-39}$Thr18p. The less negative ΔC_p observed for binding of $p53_{2-39}$Ser15p, Thr18p to Taz2 (Table 2) suggests an increase in electrostatic interactions in this complex and/or a decrease in the extent of hydrophobic interactions, possibly due to conformational restriction imposed by the two modifications. Thus, the structural and thermodynamic data suggest a means for modulation of the interaction of Taz2 and p53 TAD1 upon p53 phosphorylation.

The interaction between p53 and the Taz2 domain of p300 is crucial for p53 activity, and biological experiments have shown that phosphorylation modulates this interaction (Avantaggiati et al. 1997). The increased affinity for Taz2 upon p53 phosphorylation may amplify the p53 response through repression of alternate signaling pathways. Following DNA damage-induced p53 phosphorylation, the increased affinity of p53 for p300 may reduce the interaction of p300 with other transcription factors through competition, thereby decreasing their activity while increasing that of p53. Acetylation of p53 by p300 may further enhance this affect by promoting coactivator recruitment by p53 and subsequent histone acetylation (Barlev et al. 2001). This mechanism of repression by p53 would allow for amplification of the p53 response to DNA damage, an effect necessary to elicit cell cycle arrest or apoptosis.

Additionally, phosphorylation p53 on Thr_{18} results in weaker binding to MDM2, disrupting the MDM2/p53 complex and allowing p53 to recruit p300.

The structural studies presented here describe the molecular determinants of the binding of p53 TAD1 to the Taz2 domain of p300, a crucial interaction for p53-mediated transcriptional activation. The interaction is stabilized in part by hydrophobic interactions, mediated by Phe_{19}, Leu_{22}, and Leu_{25}. In addition, the extent of hydrophobic interaction is also increased upon p53 phosphorylation at either Ser_{15} or Thr_{18}, suggesting a possible rearrangement of the interaction with the phosphorylated protein as compared with the unmodified form. These vital modifications control the response of p53 following DNA damage by modulating its affinity for other proteins and thereby controlling whether it is degraded or stabilized and activated. Thus, details of how post-translational modifications regulate the protein-protein interactions of p53 at the molecular level are required to fully understand its functions.

Methods

Expression and Purification of Recombinant Proteins

The cloning, expression, and purification of Taz2(A_{1723}-K_{1812}/C1738A, C1746A, C1789A, C1790A) has been previously described (Jenkins et al. 2009 Biochemistry DOI:10.1021/bi801716h); this protein contains alanine mutations of four cysteine residues not involved in zinc-coordination and maintains similar secondary structure and p53-binding characteristics as the wild type protein, as expected from the characteristics of the similarly mutated Taz2 domain of CBP (De Guzman et al. 2000). Site-directed mutagenesis of Taz2 was performed using the QuikChange Mutagenesis Kit (Stratagene). Uniformly (>98%) ^{15}N-labeled or ^{15}N/^{13}C-labeled Taz2 was prepared in Celtone media (Spectra Stable Isotopes) supplemented with ^{15}N ammonium chloride and $^{13}C_6$-D-glucose as the sole nitrogen and carbon source, respectively. The coding sequence for $p53_{2-39}$ was PCR amplified from a mammalian vector containing p53 cDNA using the following primers: 5′-TGG ATC CGA GGA GCC GCA GTC AGA T-3′ and 5′-GGA ATT CTC ATG CTT GGG ACG GCA AG-3′. The amplified coding sequence was subcloned into pGEX4T-1 (GE Healthcare) using the BamHI and EcoRI restriction sites. GST-$p53_{2-39}$ was grown in *E. coli* in LB or minimal media containing ^{15}N-ammonium chloride and ^{13}C-glucose as the sole nitrogen and carbon sources, respectively. The cultures were grown at 37 °C to OD_{600} ~0.6 and induced with 0.5 mM IPTG for 3 h. The cells were spun down and resuspended in 50 mM Tris-HCl (pH 8), 120 mM NaCl, 0.5% NP-40, and 2 mM DTT (EBC buffer) and protease inhibitors (Roche Applied Science). The resuspended cells were lysed by French pressure cell and spun at 13,000×g for 1 h. The supernatant was incubated 16 h at 4 °C with glutathione sepharose (GE Healthcare) equilibrated with EBC buffer, and the bound fusion protein washed with EBC, re-equilibrated in PBS, and digested with 100 U thrombin (EMD Biosciences) for 4 h at 25 °C. The cleaved protein was further purified to >95% purity using reversed-phase high-performance liquid chromatography (RP-HPLC) on a C-18 column with 0.05% TFA/water/acetonitrile. The mass of the protein was confirmed by matrix-assisted laser desorption ionization time-of-flight (MALDI-TOF) mass spectrometry (Waters).

Peptide Synthesis

Peptides were synthesized by the solid phase method with 9-fluorenylmethoxycarbonyl (Fmoc) chemistry. Phosphoamino acids were coupled as Fmoc-Thr[PO(OBzl)OH]-OH and Fmoc-Ser [PO(OBzl)OH]-OH (Novabiochem). Fluorescence labeling of the peptide was achieved with 3 equivalents of 5-(6)-carboxyfluorescein succiniimidyl ester (Molecular Probes) in dimethylsulfoxide stirred overnight at 25 °C in the dark. The peptides were cleaved with a solution of 82.5% trifluoroacetic acid (TFA), 5% phenol, 5% thioanisole, 5% water, and 2.5%

ethandithiol, and then purified to > 95% purity by RP-HPLC on a C-4 column with 0.05% TFA/water/acetonitrile and masses confirmed by MALDI-TOF mass spectrometry (Waters).

NMR Spectroscopy

All NMR experiments were carried out at 35 °C and pH 6.3 (50 mM MES, 200 mM NaCl, 0.1 mM ZnCl, 1 mM DTT) on a Bruker 500 MHz spectrometer equipped with pulsed-field gradient units and triple resonance probes. Chemical shifts (^{1}H, ^{15}N, and ^{13}C) and NOEs of Taz2 and p53$_{2-39}$ were determined by performing standard triple-resonance experiments (Bax and Grzesiek 1993). Intermolecular NOEs were obtained from ^{15}N-edited NOESY experiments on ^{15}N, ^{2}H/^{1}H-labeled p53$_{2-39}$ complexed with Taz2. NMR data were processed with NMRPipe/NMRDraw (Delaglio et al. 1995), and analyzed with NMRView (Johnson and Blevins 1994). To confirm the NOEs, mutations and site-directed paramagnetic spin-labeling in p53$_{2-39}$ were used to identify the neighboring residues of the mutation site. Heteronuclear ^{15}N-{^{1}H} NOE experiments and analysis of the results were performed as described previously (Feng et al. 2005).

Structure Calculations

The NOE-derived restraints were subdivided into four classes, strong (1.8–2.7 Å), medium (1.8–3.3 Å), weak (1.8–5.0 Å), and very weak (1.8–6.0 Å), by comparison with NOEs of protons separated by known distances. An additional 0.5 Å was added to the upper distance limit for methyl protons and 0.2 Å was added to the upper distance limit for NH protons if the NOEs were in the strong and medium classes. Backbone dihedral angle restraints (φ and ψ angles) were obtained from analysis of ^{1}H$_\alpha$, HN, ^{13}C$_\alpha$, ^{13}C$_\beta$, ^{13}CO, and ^{15}N chemical shifts using the program TALOS (Cornilescu et al. 1999). Two constraints per hydrogen bond ($d_{NH-O} \leq 2.2$ Å and $d_{N-O} \leq 3.2$ Å) were added in the final structure calculation after initial NOE-derived structures were obtained. Structures were calculated using conjoined rigid body/ torsion angle simulated annealing with the program Xplor-NIH (Cornilescu et al. 2002, Schwieters and Clore 2001, Schwieters et al. 2003). Zn^{2+} ions were not included in the structure calculation. The quality of the 20 lowest-energy structures was analyzed by using the programs PROCHECK_NMR and MolProbity (Davis et al. 2007, Laskowski et al. 1996). Calculation of the buried surface area was performed using Surface Racer 5.0 (Tsodikov et al. 2002); the accessible surface area for helical residues of p53 were replaced with the reported median accessibilities for random coil conformations (Lins et al. 2003). Molecular graphics images were produced using the UCSF Chimera package (Pettersen et al. 2004) and DSViewer 2.0 (Accelrys).

Fluorescence Polarization Binding Assay

Taz2 (0.001 – 100 μM) was incubated with 10 nM fluorescein-labeled p53$_{14-28}$ in 20 mM acetate buffer (pH 6.0), 200 mM NaCl, 5% glycerol, 3.0 equivalents ZnCl$_2$, and 0.1 mg/ml BSA 1 h at 25 °C. Fluorescence anisotropy was measured at 25 °C on a Beacon 2000 (PanVera). The equilibrium association constant K_s, was estimated by nonlinear curve fitting of the observed anisotropies using Origin software (MicroCal). Equilibrium association constants for the binding of non-labeled p53 peptides to Taz2 were determined by a fluorescence anisotropy competition assay. p53 peptides (0.001-300 μM), 1.0 μM Taz2 and 10 nM fluorescein-labeled p53$_{14-28}$ peptide were incubated 1 h at 25 °C in 10 mM acetate buffer (pH 6.0), 200 mM NaCl, 5% glycerol, 6 μM ZnCl$_2$, and 0.1 mg/ml BSA. The equilibrium dissociation constants, K_d, were estimated by nonlinear curve fitting of the observed anisotropies.

Isothermal titration calorimetry (ITC)

ITC measurements were performed using a VP-ITC calorimeter (MicroCal). Most titrations were performed in 20 mM Tris-HCl (pH 7.5), 100 mM NaCl, and 2 mM β-mercaptoethanol at

15, 25, or 35 °C as specified. Experiments to determine the effect of salt concentration on binding were performed at 35 °C in 20 mM Tris-HCl (pH 7.5), 2 mM β-mercaptoethanol, and 50, 100, or 200 mM NaCl, as specified. The protein and peptide solutions were degassed before each experiment. Heats of dilution were subtracted from the raw data. ITC experiments with $p53_{1-39}$ phosphopeptides binding to Taz2 were fit with a 1:1 binding model using Origin software with the ITC package (Microcal). All experiments were performed at least two times.

Supplementary Material

Refer to Web version on PubMed Central for supplementary material.

Acknowledgments

References

Appella E, Anderson CW. Post-translational modifications and activation of p53 by genotoxic stresses. Eur J Biochem 2001;268:2764–2772. [PubMed: 11358490]

Avantaggiati ML, Ogryzko V, Gardner K, Giordano A, Levine AS, Kelly K. Recruitment of p300/CBP in p53-dependent signal pathways. Cell 1997;89:1175–1184. [PubMed: 9215639]

Baldwin RL. Temperature dependence of the hydrophobic interaction in protein folding. Proc Natl Acad Sci U S A 1986;83:8069–8072. [PubMed: 3464944]

Barlev NA, Liu L, Chehab NH, Mansfield K, Harris KG, Halazonetis TD, Berger SL. Acetylation of p53 activates transcription through recruitment of coactivators/histone acetyltransferases. Mol Cell 2001;8:1243–1254. [PubMed: 11779500]

Bax AD, Grzesiek S. Methodological advances in protein NMR. Accounts of Chemical Research 1993;26:131–138.

Bochkareva E, Kaustov L, Ayed A, Yi GS, Lu Y, Pineda-Lucena A, Liao JC, Okorokov AL, Milner J, Arrowsmith CH, et al. Single-stranded DNA mimicry in the p53 transactivation domain interaction with replication protein A. Proc Natl Acad Sci U S A 2005;102:15412–15417. [PubMed: 16234232]

Bottger V, Bottger A, Garcia-Echeverria C, Ramos YF, van der Eb AJ, Jochemsen AG, Lane DP. Comparative study of the p53-mdm2 and p53-MDMX interfaces. Oncogene 1999;18:189–199. [PubMed: 9926934]

Candau R, Scolnick DM, Darpino P, Ying CY, Halazonetis TD, Berger SL. Two tandem and independent sub-activation domains in the amino terminus of p53 require the adaptor complex for activity. Oncogene 1997;15:807–816. [PubMed: 9266967]

Cornilescu G, Delaglio F, Bax A. Protein backbone angle restraints from searching a database for chemical shift and sequence homology. J Biomol NMR 1999;13:289–302. [PubMed: 10212987]

Cornilescu G, Lee BR, Cornilescu CC, Wang G, Peterkofsky A, Clore GM. Solution structure of the phosphoryl transfer complex between the cytoplasmic A domain of the mannitol transporter IIMannitol and HPr of the Escherichia coli phosphotransferase system. J Biol Chem 2002;277:42289–42298. [PubMed: 12202490]

Craig AL, Burch L, Vojtesek B, Mikutowska J, Thompson A, Hupp TR. Novel phosphorylation sites of human tumour suppressor protein p53 at Ser20 and Thr18 that disrupt the binding of mdm2 (mouse double minute 2) protein are modified in human cancers. Biochem J 1999;342(Pt 1):133–141. [PubMed: 10432310]

Das S, Boswell SA, Aaronson SA, Lee SW. P53 promoter selection: choosing between life and death. Cell Cycle 2008;7:154–157. [PubMed: 18212532]

Davis IW, Leaver-Fay A, Chen VB, Block JN, Kapral GJ, Wang X, Murray LW, Arendall WB 3rd, Snoeyink J, Richardson JS, et al. MolProbity: all-atom contacts and structure validation for proteins and nucleic acids. Nucleic Acids Res 2007;35:W375–383. [PubMed: 17452350]

De Guzman RN, Liu HY, Martinez-Yamout M, Dyson HJ, Wright PE. Solution structure of the TAZ2 (CH3) domain of the transcriptional adaptor protein CBP. J Mol Biol 2000;303:243–253. [PubMed: 11023789]

Delaglio F, Grzesiek S, Vuister GW, Zhu G, Pfeifer J, Bax A. NMRPipe: a multidimensional spectral processing system based on UNIX pipes. J Biomol NMR 1995;6:277–293. [PubMed: 8520220]

Di Lello P, Jenkins LMM, Jones TN, Nguyen BD, Hara T, Yamaguchi H, Dikeakos JD, Appella E, Legault P, Omichinski JG. Structure of the Tfb1/p53 complex: Insights into the interaction between the p62/Tfb1 subunit of TFIIH and the activation domain of p53. Mol Cell 2006;22:731–740. [PubMed: 16793543]

Dunker AK, Cortese MS, Romero P, Iakoucheva LM, Uversky VN. Flexible nets. The roles of intrinsic disorder in protein interaction networks. Febs J 2005;272:5129–5148. [PubMed: 16218947]

Espinosa JM, Emerson BM. Transcriptional regulation by p53 through intrinsic DNA/chromatin binding and site-directed cofactor recruitment. Mol Cell 2001;8:57–69. [PubMed: 11511360]

Feng H, Zhou Z, Bai Y. A protein folding pathway with multiple folding intermediates at atomic resolution. Proc Natl Acad Sci U S A 2005;102:5026–5031. [PubMed: 15793003]

Goodman RH, Smolik S. CBP/p300 in cell growth, transformation, and development. Genes Dev 2000;14:1553–1577. [PubMed: 10887150]

Grossman SR, Perez M, Kung AL, Joseph M, Mansur C, Xiao ZX, Kumar S, Howley PM, Livingston DM. p300/MDM2 complexes participate in MDM2-mediated p53 degradation. Mol Cell 1998;2:405–415. [PubMed: 9809062]

Gu W, Roeder RG. Activation of p53 sequence-specific DNA binding by acetylation of the p53 C-terminal domain. Cell 1997;90:595–606. [PubMed: 9288740]

Hsu CH, Chang MD, Tai KY, Yang YT, Wang PS, Chen CJ, Wang YH, Lee SC, Wu CW, Juan LJ. HCMV IE2-mediated inhibition of HAT activity downregulates p53 function. Embo J 2004;23:2269–2280. [PubMed: 15141169]

Ito A, Lai CH, Zhao X, Saito S, Hamilton MH, Appella E, Yao TP. p300/CBP-mediated p53 acetylation is commonly induced by p53-activating agents and inhibited by MDM2. EMBO J 2001;20:1331–1340. [PubMed: 11250899]

Johnson BA, Blevins RA. NMR View: A computer program for the visualization and analysis of NMR data. J Biomol NMR 1994;4:603–614.

Kussie PH, Gorina S, Marechal V, Elenbaas B, Moreau J, Levine AJ, Pavletich NP. Structure of the MDM2 oncoprotein bound to the p53 tumor suppressor transactivation domain. Science 1996;274:948–953. [PubMed: 8875929]

Laskowski RA, Rullmannn JA, MacArthur MW, Kaptein R, Thornton JM. AQUA and PROCHECK-NMR: programs for checking the quality of protein structures solved by NMR. J Biomol NMR 1996;8:477–486. [PubMed: 9008363]

Lee H, Mok KH, Muhandiram R, Park KH, Suk JE, Kim DH, Chang J, Sung YC, Choi KY, Han KH. Local structural elements in the mostly unstructured transcriptional activation domain of human p53. J Biol Chem 2000;275:29426–29432. [PubMed: 10884388]

Lee HJ, Srinivasan D, Coomber D, Lane DP, Verma CS. Modulation of the p53-MDM2 interaction by phosphorylation of Thr18: a computational study. Cell Cycle 2007;6:2604–2611. [PubMed: 17957142]

Lins L, Thomas A, Brasseur R. Analysis of accessible surface of residues in proteins. Protein Sci 2003;12:1406–1417. [PubMed: 12824487]

Liu G, Xia T, Chen X. The activation domains, the proline-rich domain, and the C-terminal basic domain in p53 are necessary for acetylation of histones on the proximal p21 promoter and interaction with p300/CREB-binding protein. J Biol Chem 2003;278:17557–17565. [PubMed: 12609999]

Livingstone JR, Spolar RS, Record MT Jr. Contribution to the thermodynamics of protein folding from the reduction in water-accessible nonpolar surface area. Biochemistry 1991;30:4237–4244. [PubMed: 2021617]

Loladze VV, Ermolenko DN, Makhatadze GI. Heat capacity changes upon burial of polar and nonpolar groups in proteins. Protein Sci 2001;10:1343–1352. [PubMed: 11420436]

Luo J, Nikolaev AY, Imai S, Chen D, Su F, Shiloh A, Guarente L, Gu W. Negative control of p53 by Sir2alpha promotes cell survival under stress. Cell 2001;107:137–148. [PubMed: 11672522]

Meszaros B, Tompa P, Simon I, Dosztanyi Z. Molecular principles of the interactions of disordered proteins. J Mol Biol 2007;372:549–561. [PubMed: 17681540]

Pettersen EF, Goddard TD, Huang CC, Couch GS, Greenblatt DM, Meng EC, Ferrin TE. UCSF Chimera--a visualization system for exploratory research and analysis. J Comput Chem 2004;25:1605–1612. [PubMed: 15264254]

Picksley SM, Vojtesek B, Sparks A, Lane DP. Immunochemical analysis of the interaction of p53 with MDM2;--fine mapping of the MDM2 binding site on p53 using synthetic peptides. Oncogene 1994;9:2523–2529. [PubMed: 8058315]

Polley S, Guha S, Kar S, Roy NS, Sakaguchi K, Chuman Y, S V, Kundu T, Roy S. Differential recognition of phosphorylated transactivation domains of p53 by different p300 domains. J Mol Biol 2008;376:8–12. [PubMed: 18155245]

Popowicz GM, Czarna A, Holak TA. Structure of the human Mdmx protein bound to the p53 tumor suppressor transactivation domain. Cell Cycle 2008;7:2441–2443. [PubMed: 18677113]

Prabhu NV, Sharp KA. Heat capacity in proteins. Annu Rev Phys Chem 2005;56:521–548. [PubMed: 15796710]

Sakaguchi K, Herrera JE, Saito S, Miki T, Bustin M, Vassilev A, Anderson CW, Appella E. DNA damage activates p53 through a phosphorylation-acetylation cascade. Genes Dev 1998;12:2831–2841. [PubMed: 9744860]

Sakaguchi K, Saito S, Higashimoto Y, Roy S, Anderson CW, Appella E. Damage-mediated phosphorylation of human p53 threonine 18 through a cascade mediated by a casein 1-like kinase. Effect on Mdm2 binding. J Biol Chem 2000;275:9278–9283. [PubMed: 10734067]

Schwieters CD, Clore GM. Internal coordinates for molecular dynamics and minimization in structure determination and refinement. J Magn Reson 2001;152:288–302. [PubMed: 11567582]

Schwieters CD, Kuszewski JJ, Tjandra N, Clore GM. The Xplor-NIH NMR molecular structure determination package. J Magn Reson 2003;160:65–73. [PubMed: 12565051]

Scolnick DM, Chehab NH, Stavridi ES, Lien MC, Caruso L, Moran E, Berger SL, Halazonetis TD. CREB-binding protein and p300/CBP-associated factor are transcriptional coactivators of the p53 tumor suppressor protein. Cancer Res 1997;57:3693–3696. [PubMed: 9288775]

Smart JL, McCammon JA. Phosphorylation stabilizes the N-termini of alpha-helices. Biopolymers 1999;49:225–233. [PubMed: 9990840]

Teufel DP, Freund SM, Bycroft M, Fersht AR. Four domains of p300 each bind tightly to a sequence spanning both transactivation subdomains of p53. Proc Natl Acad Sci U S A 2007;104:7009–7014. [PubMed: 17438265]

Tsodikov OV, Record MT Jr, Sergeev YV. Novel computer program for fast exact calculation of accessible and molecular surface areas and average surface curvature. J Comput Chem 2002;23:600–609. [PubMed: 11939594]

Vaziri H, Dessain SK, Ng Eaton E, Imai SI, Frye RA, Pandita TK, Guarente L, Weinberg RA. hSIR2 (SIRT1) functions as an NAD-dependent p53 deacetylase. Cell 2001;107:149–159. [PubMed: 11672523]

Vise P, Baral B, Stancik A, Lowry DF, Daughdrill GW. Identifying long-range structure in the intrinsically unstructured transactivation domain of p53. Proteins 2007;67:526–530. [PubMed: 17335006]

Vise PD, Baral B, Latos AJ, Daughdrill GW. NMR chemical shift and relaxation measurements provide evidence for the coupled folding and binding of the p53 transactivation domain. Nucleic Acids Res 2005;33:2061–2077. [PubMed: 15824059]

Wishart DS, Bigam CG, Holm A, Hodges RS, Sykes BD. 1H, 13C and 15N random coil NMR chemical shifts of the common amino acids. I. Investigations of nearest-neighbor effects. J Biomol NMR 1995;5:67–81. [PubMed: 7881273]
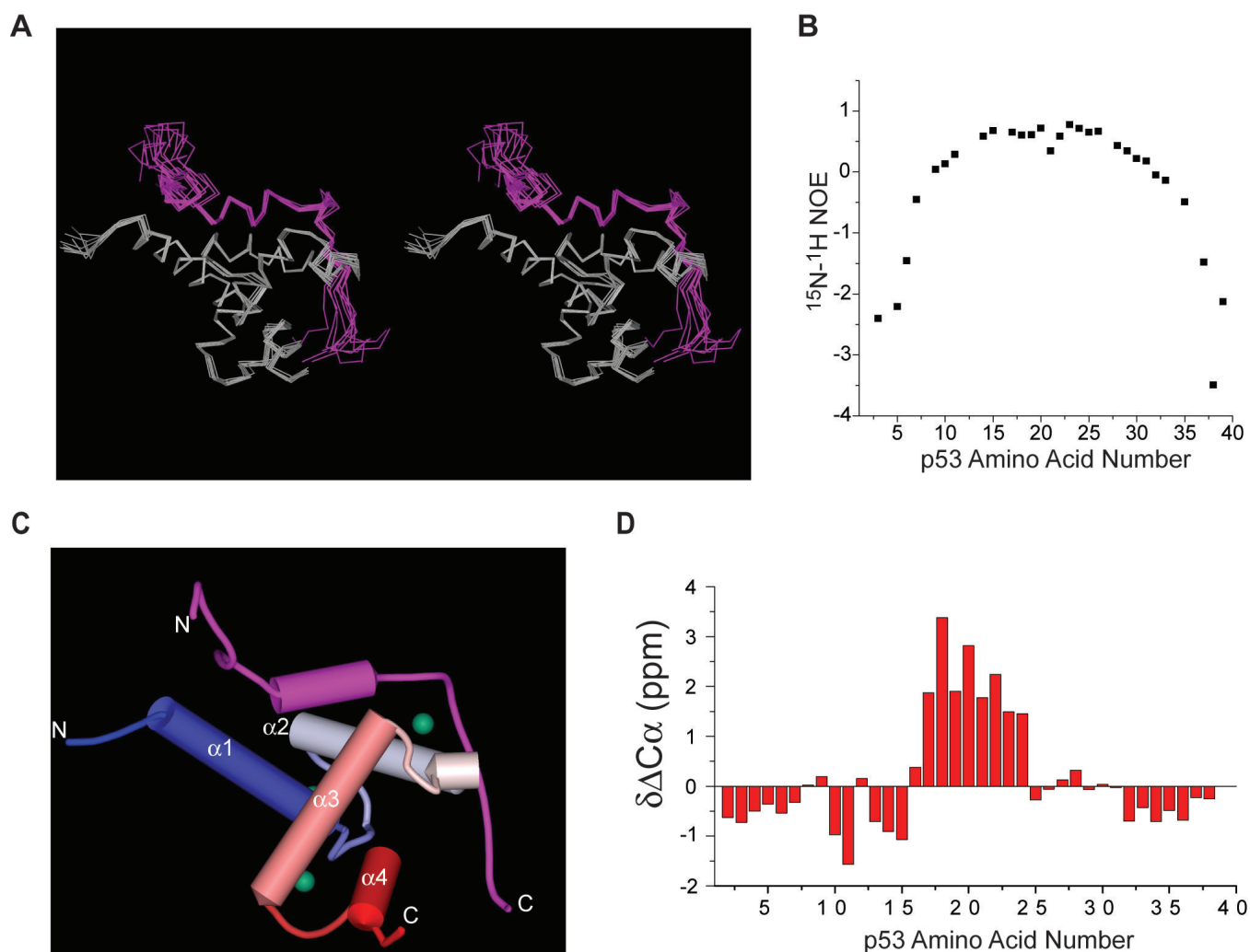
A

B

C

D

Figure 1. Structure of the Taz2-p53$_{2\text{-}39}$ Complex

(**A**) Stereo image of the overlay of 10 lowest-energy NMR structures of the complex between p53$_{15\text{-}27}$ (purple) and the Taz2 domain of p300 (gray). The structures are superimposed on the Cα traces. (**B**) Plot of backbone amide ^{15}N-{^{1}H} heteronuclear NOEs of p53$_{2\text{-}39}$. (**C**) Cylinder model of the average conformation of the complex. p53 is shown in magenta and the helices of Taz2 are shown in blue (α1), lilac (α2), orange (α3), and red (α4). Zinc ions in Taz2, modeled as green spheres, were added according to zinc-coordination distances into the known binding cage. (**D**) Secondary chemical shift difference of p53$_{2\text{-}39}$ in the complex (measured Cα chemical shift – random coil value).
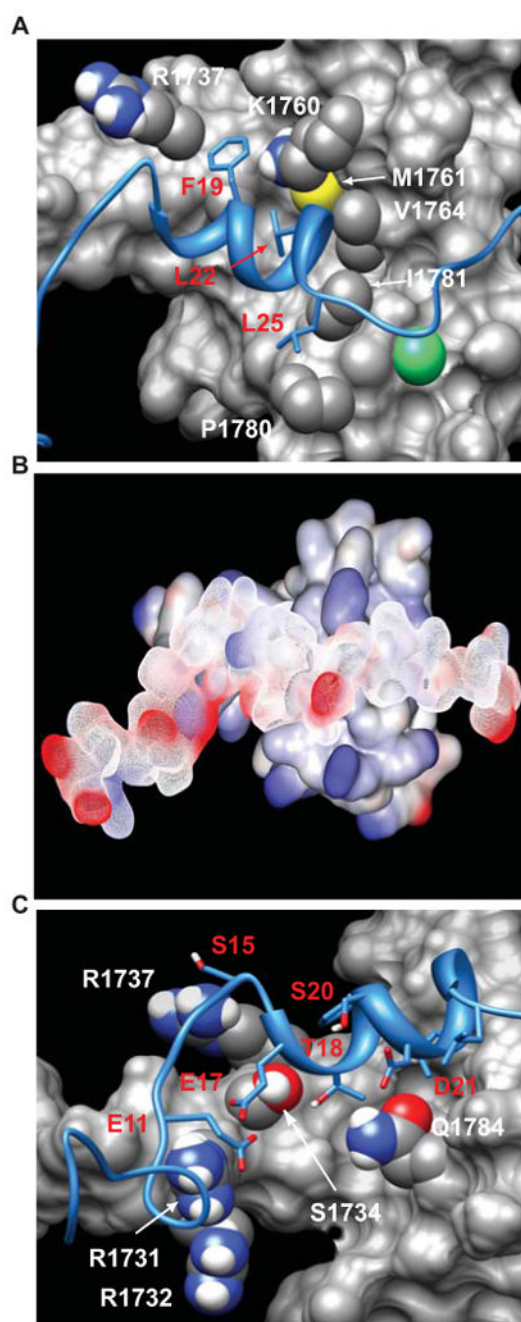
Figure 2. Stabilizing Interactions between p53$_{2-39}$ and Taz2

(**A**) Model of the Taz2-p53$_{2-39}$ complex, showing residues that make hydrophobic contacts. Contacting residues are labeled in white for Taz2 (gray surface representation) and red for p53$_{2-39}$ (blue ribbon). (**B**) Model of the Taz2-p53$_{2-39}$ complex, colored by electrostatic potential (red – negative, blue – positive). Taz2 is shown in a solid representation, and p53$_{2-39}$ as a mesh. (**C**) Model of the Taz2-p53$_{2-39}$ complex, showing residues that make electrostatic contacts. Contacting residues are labeled in white for Taz2 (gray surface representation) and red for p53$_{2-39}$ (blue ribbon).
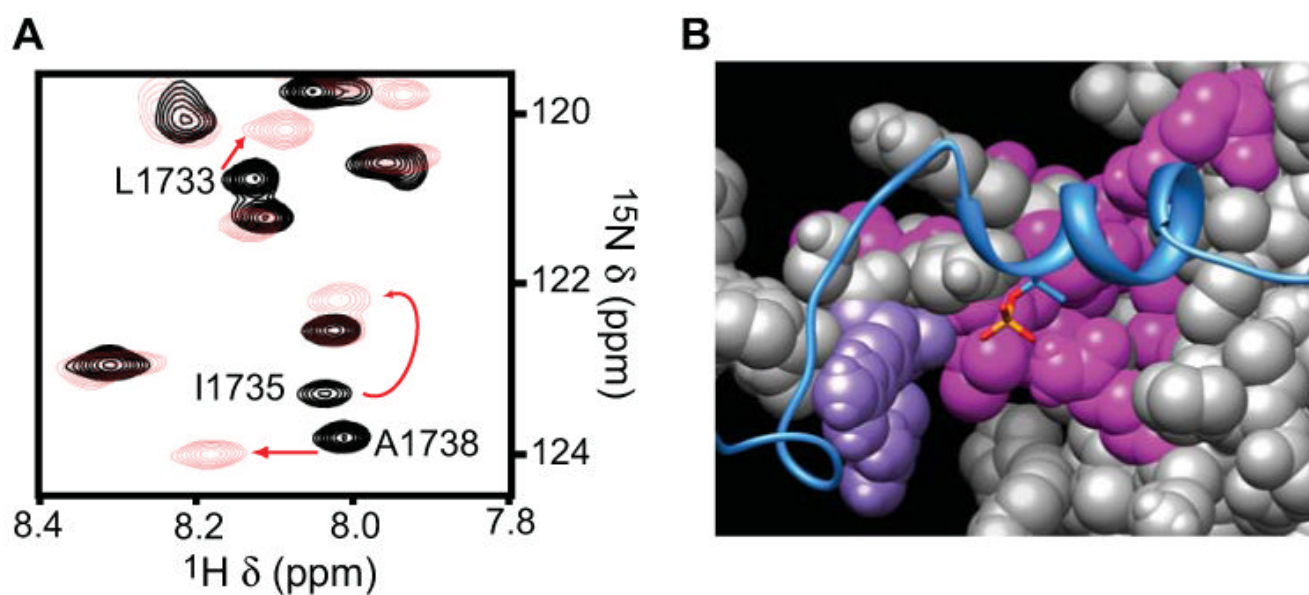
Figure 3. Effect of p53 Phosphorylation on Taz2 Conformation
(**A**) Overlay of a selected region of 2D ^{1}H,^{15}N HSQC spectra of ^{15}N-labeled Taz2 complexed with p53$_{2-39}$ (black) and in complex with p53$_{1-39}$Thr18p (red). (**B**) Model of Taz2-p53$_{2-39}$ complex showing residues with significant changes in their amide chemical shifts upon addition of p53$_{1-39}$Thr18p. Residues of Taz2 (space-fill) with chemical shift changes shown in magenta; the two nearby arginine residues of Taz2 are shown in purple. The side chain of Thr$_{18}$ of p53 (blue ribbon) is shown as sticks.

Table 1

Parameters for the NMR Structures

NMR distance and dihedral constraints	
Total NOE	1732
Intra residues NOE	521
Sequential NOE ($|i-j|=1$)	499
Short range NOE ($|i-j|\leq4$)	473
Long range NOE ($|i-j|\geq5$)	253
Inter-protein NOE	52
H-bonds	94
Dihedral angles	229
Structure statistics	
Violations (mean ± s.d.)	
NOE(all) (Å)	0.050 ± 0.003
Dihedral (°)	0.506 ± 0.025
Max. dihedral angle violation (°)	3.58
Max. distance constraint violation (Å)	0.33
Deviations from idealized geometry	
Bonds (Å)	0.0052 ± 0.0005
Angles (°)	0.724 ± 0.036
Impropers (°)	0.577 ± 0.026
Average pairwise r.m.s. deviation (Å)	
All heavy atoms (Å)	0.56
Backbone atoms (Å)	0.31
Ramachandran plots	
Most favored regions	$88.9\% \pm 1.0$
Allowed regions	$8.7\% \pm 1.1$
Generously allowed regions	0.0 ± 0.0
Disallowed regions	$2.4\% \pm 0.2$
Molprobity results	
Clashscore, all atom	27.91
Rotamer outliers	5.06%
Ramachandran outliers	8.35%
Ramachandran favored	84.0%
Molprobity score	3.13
Residues with bad bonds	0.0%
Residues with bad angles	0.0%

Residues 1727-1810 in Taz2 and 15-27 in TAD1 were used to calculate the structural statistics. The 20 lowest-energy structures were used in the calculation.

Table 2

Thermodynamic constants for the binding of Taz2 to phosphorylated forms of p53$_{1-39}$.[a]

		p53$_{1-39}$Ser15p	p53$_{1-39}$Thr18p	p53$_{1-39}$Ser15p, Thr18p
$K_d(\mu M)$	15 °C	0.49 ± 0.17	0.40 ± 0.15	0.20 ± 0.07
	35 °C	0.96 ± 0.26	0.23 ± 0.03	0.41 ± 0.09
ΔH (kcal/mol)	15 °C	3.91 ± 0.24	4.01 ± 0.22	1.55 ± 0.06
	35 °C	-4.68 ± 0.45	-4.14 ± 0.36	-2.28 ± 0.44
ΔS (EU)[b]	15 °C	42.5 ± 0.1	43.3 ± 0.1	36.2 ± 0.9
	35 °C	12.4 ± 0.9	16.9 ± 1.4	21.9 ± 0.4
ΔG (kcal/mol)	15 °C	-8.34 ± 0.20	-8.44 ± 0.20	-8.86 ± 0.21
	35 °C	-8.48 ± 0.17	-9.35 ± 0.07	-9.03 ± 0.31
ΔC_p (cal/mol·K)		-429	-408	-192

[a]Thermodynamic constants were determined by ITC.

[b]Entropy units.

Table 3

Dissociation constants (µM) for binding of Taz2 to $p53_{1-39}$ or its phosphorylated forms at two salt concentrations.[a]

	50 mM	200 mM
$p53_{1-39}$	0.43 ± 0.30	7.15 ± 3.62
$p53_{1-39}$Ser15p	0.04 ± 0.01	1.83 ± 0.23
$p53_{1-39}$Thr18p	0.05 ± 0.01	1.05 ± 0.16
$p53_{1-39}$Ser15p, Thr18p	0.05 ± 0.00	1.74 ± 0.81

[a]Dissociation constants were determined by ITC at 35 °C.

Table 4

Dissociation constants for binding of Taz2 mutants to p53$_{1-39}$ or its phosphorylated forms (μM).[a]

	Taz2	Taz2 R1731A	Taz2 R1732A	Taz2 R1737A
p53$_{1-39}$	2.7 ± 0.5	3.5 ± 1.1	3.7 ± 1.0	3.6 ± 1.1
p53$_{1-39}$ Ser15p	0.96 ± 0.26	ND	ND	0.91 ± 0.12
p53$_{1-39}$ Thr18p	0.23 ± 0.03	0.72 ± 0.16	0.68 ± 0.01	ND

[a]Dissociation constants were determined by ITC at 35 °C.